High quality InSAR data linked to seasonal change in hydraulic head for an agricultural area in the San Luis Valley, Colorado

Jessica A. Reeves,[1] Rosemary Knight,[1] Howard A. Zebker,[1] Willem A. Schreüder,[2] Piyush Shanker Agram,[3] and Tom R. Lauknes[4]

Received 7 December 2010; revised 20 September 2011; accepted 19 October 2011; published 14 December 2011.

[1] In the San Luis Valley (SLV), Colorado legislation passed in 2004 requires that hydraulic head levels in the confined aquifer system stay within the range experienced in the years 1978–2000. While some measurements of hydraulic head exist, greater spatial and temporal sampling would be very valuable in understanding the behavior of the system. Interferometric synthetic aperture radar (InSAR) data provide fine spatial resolution measurements of Earth surface deformation, which can be related to hydraulic head change in the confined aquifer system. However, change in cm-scale crop structure with time leads to signal decorrelation, resulting in low quality data. Here we apply small baseline subset (SBAS) analysis to InSAR data collected from 1992 to 2001. We are able to show high levels of correlation, denoting high quality data, in areas between the center pivot irrigation circles, where the lack of water results in little surface vegetation. At three well locations we see a seasonal variation in the InSAR data that mimics the hydraulic head data. We use measured values of the elastic skeletal storage coefficient to estimate hydraulic head from the InSAR data. In general the magnitude of estimated and measured head agree to within the calculated error. However, the errors are unacceptably large due to both errors in the InSAR data and uncertainty in the measured value of the elastic skeletal storage coefficient. We conclude that InSAR is capturing the seasonal head variation, but that further research is required to obtain accurate hydraulic head estimates from the InSAR deformation measurements.

Citation: Reeves, J. A., R. Knight, H. A. Zebker, W. A. Schreüder, P. Shanker Agram, and T. R. Lauknes, (2011), High quality InSAR data linked to seasonal change in hydraulic head for an agricultural area in the San Luis Valley, Colorado, *Water Resour. Res.*, *47*, W12510, doi:10.1029/2010WR010312.

1. Introduction

[2] The San Luis Valley (SLV) is an 8000 km^2 high-altitude valley, located mostly on the northern side of the Colorado–New Mexico border. The Rio Grande River runs through the center of the SLV to the downstream states of New Mexico and Texas. Legislation passed in 2004 established that hydraulic head levels within the confined aquifer system should be maintained within the range experienced in the years between 1978 and 2000. What is required in the SLV is the ability to manage the various demands for water while ensuring the long-term sustainability of the groundwater system.

[3] The Colorado Water Conservation Board and the Colorado Division of Water Resources have developed the Rio Grand Decision Support System (RGDSS), a project run by a number of cooperating organizations to quantitatively study the water resources in the SLV. The RGDSS includes a hydrogeologic database and a MODFLOW finite difference groundwater flow model that can be used to evaluate historic and proposed groundwater management practices, develop a groundwater budget, and identify areas for future research. While over 1500 wells with hydraulic head measurements are used to characterize the flow system and calibrate the RGDSS MODFLOW model, spatial resolution is still too coarse to adequately represent the heterogeneity of the subsurface. In addition, in numerous areas there are limited hydraulic head measurements available in the time period (1978–2000) now defined as the reference period in the groundwater legislation.

[4] A critical challenge for the RGDSS is the acquisition of sufficiently dense spatial and temporal sampling to characterize the spatially heterogeneous, time-varying behavior of the confined aquifer system in this large-scale (8000 km^2) model. Remotely sensed data can offer spatially and temporally dense measurements over very large areas, and in the case of the SLV historic measurements during the time period of interest exist. Of particular relevance to the characterization of groundwater systems is interferometric synthetic aperture radar (InSAR), a remote sensing method that maps the relative ground surface deformation.

[5] The deformation of the ground surface, which we derive here from InSAR data, is directly related to changes in the thickness of the confined aquifer due to recharge and

[1]Department of Geophysics, Stanford University, Stanford, California, USA.
[2]Principia Mathematica, Lakewood, Colorado, USA.
[3]Division of Geological & Planetary Sciences, California Institute of Technology, Pasadena, California, USA.
[4]Northern Research Institute (Norut), Tromsø Science Park, Tromsø, Norway.

0043-1397/11/2010WR010312

withdrawal of groundwater. In general the deformation caused by hydraulic head change in confined aquifer systems is much greater than for unconfined aquifer systems due to larger changes in effective stress. InSAR has been used to map the spatial extent of confined aquifer system compaction [*Galloway et al.*, 1998; *Amelung et al.*, 1999; *Hoffmann et al.*, 2001] as well as monitor compaction over time [*Schmidt and Burgmann*, 2003]. The change in aquifer thickness Δb is governed by the change in hydraulic head Δh and the elastic skeletal storage coefficient S_{ke}, a parameter that characterizes the skeletal compressibility of the aquifer system [*Riley*, 1969]:

$$\Delta b = S_{ke}\Delta h. \tag{1}$$

[6] This relationship is valid when the aquifer system is deforming elastically/recoverably. In order for an aquifer system to be deforming elastically the effective stress must be less than the preconsolidation stress, or equivalently the hydraulic head must be above the minimum historical hydraulic head. In this study we assume that Δb is equal to the deformation of the ground surface as measured by InSAR, that Δh is the change in head that would be measured in monitoring wells, and that S_{ke} can be obtained from an aquifer test.

[7] An aquifer test involves pumping water out of the aquifer system at a pumping well and inducing a drawdown of the hydraulic head at monitoring wells some distance away. We will refer to the well that the water is pumped from as the aquifer test well. Once pumping is finished the hydraulic head levels rebound. During this rebound the hydraulic head change through time is measured. This measurement is compared to the analytical solution of the hydraulic head change. The transmissivity (T) and the storage coefficient (S) that allow the analytical solution to match the measurements are the estimated aquifer parameters. In order to get an accurate measure of S at least one monitoring well must be used other than the aquifer test well. The storage coefficient S that is obtained has two components:

$$S = S_{ke} + S_w, \tag{2}$$

the elastic skeletal storage (S_{ke}) and the component of storage due to the compaction of water (S_w). In general S_w is small compared to S_{ke}, so we can assume $S_{ke} = S$: this is the assumption made throughout our study.

[8] The long-term goal of our research is to use InSAR data, which provide a level of spatial and temporal sampling that cannot readily be achieved with well measurements, to improve the reliability of the RGDSS groundwater flow model. The first step, the focus of this present study, is to determine whether we can obtain sufficiently high quality InSAR data in the SLV. The SLV is an agricultural area, where crop growth, irrigation, land erosion, and harvesting cycles can all seriously degrade the InSAR data by perturbing the positions of individual radar scatterers. In contrast, the studies noted above were all conducted in areas that have arid to semiarid climates, so changes in vegetation did not greatly interfere with the InSAR measurements. Here we use an innovative method of processing InSAR data, denoted small baseline subset (SBAS) analysis, to identify areas on the ground where the radar signals are not degraded over time. We find that we can obtain high quality InSAR data from the SLV in this way, with implications for the use of InSAR data in other agriculture areas around the world. The ability to use remotely sensed data to improve the predictability of groundwater flow models in agricultural areas would significantly advance our approach to groundwater management. The first step is to ensure that we can obtain high quality data.

2. Introduction to InSAR

2.1. InSAR Background

[9] Synthetic aperture radar (SAR) is a microwave imaging system, which uses a radar antenna mounted on an airborne or satellite-based platform to transmit and receive electromagnetic (EM) waves. The ERS-1 and ERS-2 satellites used in this study have a repeat cycle of 35 days and operate at a frequency of 5.3 GHz. The radar maps a continuous 100 km wide swath along the direction of flight, which is known as a track. In order to ease processing each track of data is divided into square frames. Each pixel in a frame contains a complex number describing the reflected amplitude and phase of the EM wave from a resolution cell on the ground, which in this study is on the order of 5 m by 25 m.

[10] Standard InSAR processing techniques combine two SAR scenes of the same area, acquired at different times. Data are collected along the line of sight (LOS) direction from the antenna to Earth's surface. The look angle is defined as the angle between the LOS and the normal to Earth's surface. For the ERS satellites the look angle is approximately 23 deg, so the change in LOS distance from the antenna to the surface is approximately equal to the change in vertical distance to the surface. The difference in the phase component ($\Delta\Phi$) of the reflected signals is known as radar interferometry [*Zebker et al.*, 1994]. If we remove the effects of topography $\Delta\Phi$ can provide an accurate measure of the change in the elevation of the land surface. Pixels are often spatially averaged to correspond to a 50 m by 50 m resolution cell to improve the signal-to-noise ratio of the observed interferometric phase. Because of the cyclic nature of phase, $\Delta\Phi$ will only be known within 2π rad; this is called the wrapped phase. The process of estimating and adding the unknown correct integer multiple of 2π to $\Delta\Phi$ is called phase unwrapping.

[11] The measured difference in the phase of the two signals $\Delta\Phi$ is the sum of four parts [*Zebker et al.*, 1994; *Ferretti et al.*, 2000]:

$$\Delta\Phi = \Delta\Phi_{\text{def}} + \Delta\Phi_{\text{topo}} + \Delta\Phi_{\text{atm}} + \Delta\Phi_n, \tag{3}$$

where $\Delta\Phi_{\text{def}}$ is the phase change due to the deformation of the ground surface, $\Delta\Phi_{\text{topo}}$ is the phase change due to topography, $\Delta\Phi_{\text{atm}}$ is the phase change due to temporal atmospheric variability, and $\Delta\Phi_n$ is other, random phase noise. $\Delta\Phi_{\text{def}}$ is related to the deformation (Δd) by

$$\Delta\Phi_{\text{def}} = \frac{2\pi}{\lambda}(2\Delta d) = \frac{4\pi}{\lambda}\Delta d, \tag{4}$$

where λ is the wavelength of the radar system. We must first remove $\Delta\Phi_{\text{topo}}$, $\Delta\Phi_{\text{atm}}$, and $\Delta\Phi_n$ in each of the

interferograms in order to determine $\Delta\Phi_{def}$. The removal of $\Delta\Phi_{topo}$ and $\Delta\Phi_{atm}$ is well documented in the literature, so we will focus on the phase noise in the measurement $\Delta\Phi_n$ [*Zebker et al.*, 1994; *Hanssen*, 2001; *Zebker et al.*, 1997; *Ferretti et al.*, 2001].

[12] The phase change due to phase noise is caused by signal decorrelation and cannot readily be compensated for without sacrificing spatial resolution. For a given pixel in an interferogram we compute the coherence as a quality measure for the phase difference $\Delta\Phi_n$ between two SAR scenes at that point. The complex coherence (γ) is defined as follows:

$$\gamma = \frac{\langle S_1 S_2^* \rangle}{\sqrt{\langle S_1 S_1^* \rangle \langle S_2 S_2^* \rangle}}, \tag{5}$$

where $\langle\ \rangle$ denotes the expected value, S_1 and S_2 are the complex values of SAR scene 1 and SAR scene 2, and S_1^* and S_2^* are the complex conjugates of SAR scene 1 and SAR scene 2 for a small sample of pixels around the pixel in question. Often the magnitude of the complex coherence is used, referred to as only the coherence, which can range from 0 to 1. We describe an interferogram as coherent/well correlated, if many of the pixels have coherence near 1; or as incoherent/decorrelated, if many of the pixels have coherence near 0.

[13] The coherence can be described as the product of the thermal coherence γ_{therm}, the spatial coherence γ_{spat}, and the temporal coherence γ_{temp} [*Zebker and Villasenor*, 1992]:

$$\gamma = \gamma_{therm} \cdot \gamma_{spat} \cdot \gamma_{temp}, \tag{6}$$

where γ_{therm} quantifies the system noise, a characteristic of the system configuration, γ_{spat} is a factor corresponding to the viewing angle of the satellite between the acquisition of the two scenes, as described above as a parallax effect. The reflection from a scattering area viewed at one angle will be different when viewed at another angle. We quantify this change in viewing angle by the spatial distance between the two satellite positions, the spatial baseline.

[14] The most difficult effect to deal with is the temporal coherence γ_{temp}. Temporal decorrelation follows from wavelength-scale changes in the positions of scatterers within each resolution cell between the acquisition times of the two scenes. The time between two scenes is called the temporal baseline; long temporal baselines tend to decrease γ_{temp}. A surface can decorrelate with time due to processes or activities such as seasonal vegetation changes, erosion of the land surface, agricultural activity, or construction. The best way to mitigate this effect is to form interferograms from scene pairs with small temporal baselines. This concept will be discussed further when we review a technique called small baseline subset analysis (SBAS) in section 3.

2.2. Groundwater Studies Using Standard InSAR Processing

[15] Standard InSAR techniques worked well in the Antelope Valley and the Las Vegas Valley because the arid climate leads to little or no temporal decorrelation [*Galloway et al.*, 1998; *Amelung et al.*, 1999]. *Amelung et al.* [1999] were able to interfere scenes with a temporal baseline of 6 years and retain coherence. Vegetated areas were masked out in their study due to low coherence. A number of studies were able to improve upon standard processing techniques by only interfering scenes with a small spatial baseline [*Galloway et al.*, 1998; *Amelung et al.*, 1999; *Hoffmann et al.*, 2001; *Watson et al.*, 2002; *Hoffmann et al.*, 2003; *Schmidt and Burgmann*, 2003; *Canuti et al.*, 2006; *Wisely and Schmidt*, 2010]. This technique produces a number of differential phase measurements. In order to construct a time series of the phase change, the interferograms were formed with a common scene, or a least-squares (LS) phase inversion was used to retrieve the phase values relative to the first scene.

[16] *Hoffmann et al.* [2001] used a time series of InSAR deformation measurements and hydraulic head measurements to estimate the elastic storage coefficient (S_{ke}) for five different positions in the Las Vegas Valley. These estimates were compared to the storage coefficient of the aquifer system ($S = S_s b^*$), computed by estimating the thickness of the aquifer system b^* and assuming a value for the specific storage, $S_s = 3 \times 10^{-6}(\mathrm{m}^{-1})$ for most producing aquifer sediments [*Todd*, 1980]. They found that S_{ke} and S agree at best within 20% and at worst by a factor of 8. *Hoffmann et al.* [2003] expanded upon their previous study by incorporating the InSAR deformation time series into a MODFLOW finite difference groundwater flow model in order to estimate the inelastic aquifer system compressibilities and improve the models ability to predict groundwater flow. The inelastic parameters estimated were able to reproduce leveling line surveys measuring surface deformation, however the predictive ability of the model was not improved.

[17] *Schmidt and Burgmann* [2003] used a LS time series analysis to assess compaction in the Santa Clara Valley, California. With 47 scenes over 8 years they were able to compare their InSAR time series to leveling data for the urban area around San Jose and along the developed coast of San Francisco Bay. They showed that the InSAR data correlated well with extensometer measurements at two sites. However, no results were possible for vegetated areas because of significant temporal decorrelation, and no work was done to try to estimate storage parameters. A more recent study by *Wisely and Schmidt* [2010] estimated storage parameters at sites where they had hydraulic head data, InSAR data, and an estimate of the thickness of the aquifer system from a basin depth model. The study was conducted in the San Bernardino basin, California, which is primarily an urban environment. Due to the lack of surface change over time, urban areas, like arid areas, do not decorrelate as quickly.

3. Small Baseline Subset (SBAS) Analysis

[18] In the SLV we are working in an agricultural area where crop growth, irrigation, land erosion, and harvesting cycles can all change the detailed shape of the imaged surface and ground cover between the acquisition of any two SAR scenes, leading to decorrelation of the signals. But in some agricultural areas stable patches have been found around farmed fields yielding InSAR data with high coherence [*Meyer et al.*, 1996; *Massonnet and Feigl*, 1998]. We wish to use these selected areas to analyze deformation in otherwise challenging terrains. A recently developed technique, small baseline subset (SBAS) analysis, combines the coherent areas in a series of interferograms to produce a

map of deformation time series [*Berardino et al.*, 2002]. Phase decorrelation is minimized by imposing constraints on the temporal and spatial baselines for each pair of scenes that are interfered. To date, this multitemporal technique has only been proven to work well in arid, semiarid, and urban areas [*Galloway and Hoffmann*, 2007]. We show here that it provides accurate deformation observations across the SLV as well.

3.1. Introduction to SBAS

[19] The basic principle underlying SBAS is proper scene selection combined with a LS analysis of the phases in the resulting unwrapped interferograms. Interferogram selection is illustrated in Figure 1, a plot of spatial versus temporal baseline for all available SAR scenes from an area. Each scene is shown as a dot with the spatial and temporal baselines plotted relative to the first scene. Lines, which signify an interferogram, connect scenes if the spatial and temporal baselines are below some selected threshold. In general, a smaller spatial baseline leads to better coherence, so we try to minimize the spatial baseline threshold for the set of interferograms. The temporal baseline threshold is dependent on how rapidly the surface properties change with time in a given area and so, for example, could be 6 years for areas in an arid climate, but a few months for vegetated areas. Each group of connected scenes is known as a small baseline subset. As long as the subsets overlap for some period of time, an LS singular value decomposition (LS SVD) can be used to solve for a time series of deformation, relative to the first scene. For the mathematical formulation of SBAS analysis see *Berardino et al.* [2002].

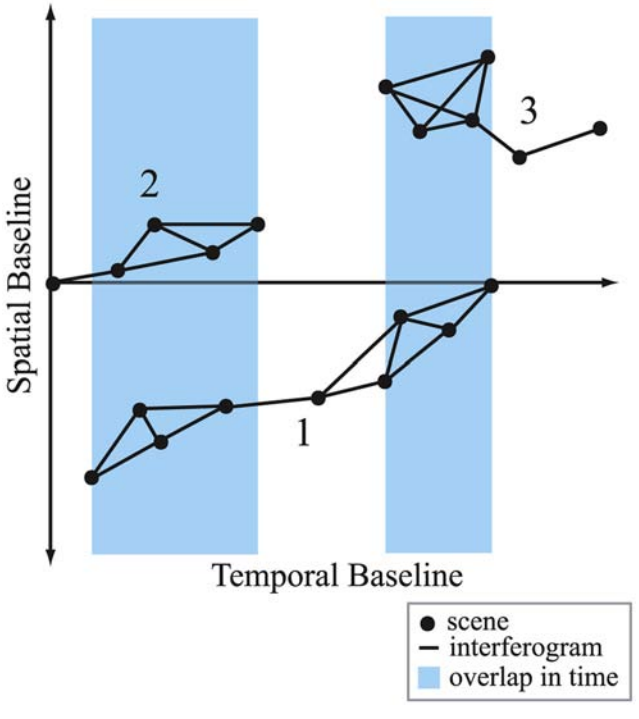

Figure 1. Example spatial versus temporal baseline plot with three small baseline subsets. Subset 1 and 2 overlap in the first blue shaded region, and subset 1 and 3 overlap in the second blue shaded region. This data set will be able to produce a time series that spans from the first scene to the last scene plotted.

3.2. Applying SBAS

[20] In this study the SBAS technique described above was implemented via the generic SAR (GSAR) software package developed by Norut [*Larsen et al.*, 2005]. We first created the spatial versus temporal baseline plot by iteratively selecting the optimal thresholds. While keeping thresholds low in order to maximize coherence we also tried to keep as many interferograms as possible, as the most accurate inversions are produced when the subsets are well connected (i.e., many interferograms are connecting scenes). We selected 400 m and 4 years, for our final spatial and temporal baseline thresholds, respectively.

[21] We then calculated the mean coherence for every pixel and applied a thresholding mask, which only allowed highly coherent pixels to be used in the remainder of the analysis. In our analysis a pixel was selected if $\gamma > 0.26$ in at least 50% of the interferograms. In the development of the SBAS method, *Berardino et al.* [2002] and *Lauknes* [2004] determined values for the thresholding mask: they set thresholds $\gamma > 0.25$ in at least 30% of the interferograms and $\gamma > 0.3$ in at least 30% of the interferograms, respectively. We found these values were too admissive for the SLV. We initially set the mask as done previously ($\gamma >$ 0.25 in at least 30% of the interferograms) and iteratively increased both γ and the percentage of the interferograms required. As these two values are increased, fewer pixels are selected. Our goal was to have a mask that would require high coherence while still selecting pixels across the entire SLV. We note that although these values seem low for a coherence threshold the fact that we are using multiple interferograms inherently reduces noise levels in the inversion. It is similar to averaging the phase noise out of the data by superimposing multiple measurements.

[22] We then removed the topographic phase and performed the phase unwrapping [*Chen and Zebker*, 2002; *Ferretti et al.*, 2007]. *Berardino et al.* [2002] used a low pass (LP) deformation model in order to further filter the data for atmospheric effects. This processing step involves prior knowledge of the deformation present. Because we know that the deformation will vary throughout the SLV and cannot be fit by a simple linear, quadratic, cubic, or sinusoidal function we decided not to implement this processing step. However, we estimated the DEM error, and subtracted that portion of the phase from each interferogram before performing the LS SVD as described in *Berardino et al.* [2002].

4. Results and Discussion

4.1. Description of SAR Data

[23] We acquired SAR data from two sources: the Western North American Interferometric Synthetic Aperture Radar Consortium (WInSAR) and the European Space Agency (ESA). For this study we used the ERS-1 and ERS-2 satellites, covering the period from 1992 to 2000. Table 1 shows the number of scenes that were acquired over the SLV. Figure 2 shows the RGDSS model boundary and the spatial extent of available scenes.

Table 1. SAR Acquisitions Over the SLV, See Figure 2 for the Location of Each Frame

Track	Frame	Scenes	Start	End
98	2853	50	1992	2008
98	2835	50	1992	2008
327	2853	23	1995	1999

[24] For this study we chose to use track 98 and frame 2853, which has 50 scenes with good spatial coverage of the valley. Scenes from 2001 to 2005 could not be used because of problems with the satellite's navigational system. For this initial assessment of data quality we focused on scenes from 1992 to 2000, which would be able to provide valuable information for the confined aquifer rules decision of 2004. We were thus limited to 31 scenes. We applied the baseline thresholds discussed in section 3.2 and produced a single subset of 89 interferograms.

4.2. Preliminary Review of Interferograms

[25] All interferograms were inspected as a preliminary review of the data. Our objective was to identify the regions in the SLV where in the interferograms alone there was evidence of deformation induced by groundwater pumping. In Figure 3, an interferogram from November 1999 to July 2000, we see a strong deformation phase signature in the southwest region of the SLV, enclosed by the red box. This pattern of concentric rings of constant phase is indicative of a subsidence bowl. The spatial distribution is consistent with the shape of a cone of depression, the drawdown of the hydraulic head around a well during pumping. Upon further investigation we found that the groundwater pumping from the confined aquifer system is relatively high in this area and the seasonal hydraulic head change is often more than 7 m. The same pattern of concentric rings was found in a number of the interferograms, and was most prominent in interferograms that spanned over a pumping season.

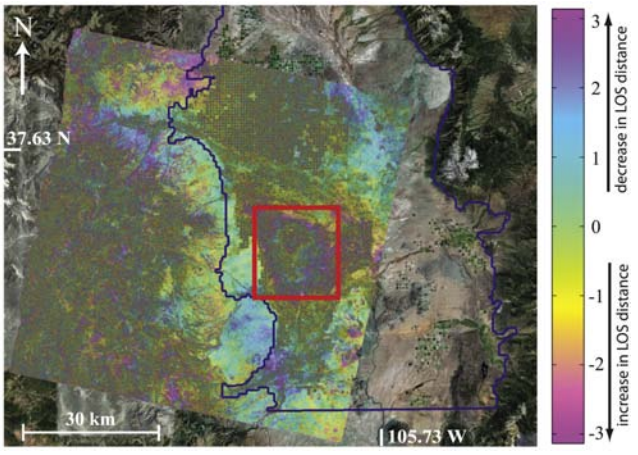

Figure 3. An interferogram from November 1999 to July 2000. The scale is in radians, where from magenta to magenta is 2π rad of phase change [source of background image: Google Earth map with Rio Grand Decision Support System (RGDSS) model boundary].

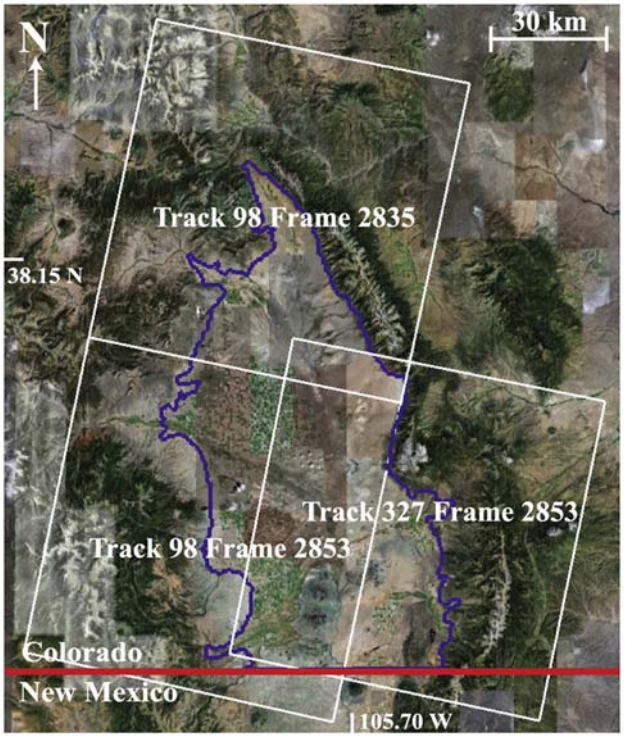

Figure 2. The RGDSS model boundary (purple), available InSAR data (white), and the state line between Colorado and New Mexico (red) (source of background image: Google Earth map with ESA track and frame overlays).

[26] This single interferogram has provided some idea of the spatial extent of the seasonal deformation. However, we still needed an estimate of the quality of the data throughout time. During the SBAS analysis we calculated the mean coherence of the InSAR data for all interferograms from 1992 to 2000.

4.3. SBAS—Discussion of the Mean Coherence

[27] The first step in undertaking SBAS analysis is to calculate the mean coherence for all pixels in all of the interferograms. Figure 4 shows the mean coherence (γ_{mean}) for all pixels. The average mean coherence value is 0.20, the maximum value is 0.92, and the minimum value is 0.10. We find that the least coherent pixels $(\gamma_{\text{mean}} < 0.2)$ fall outside the RGDSS model area in the mountainous region to the west of the SLV. The topography of this mountainous region affects the coherence if the spatial baseline is too large (i.e., the viewing angle of the two orbits is very disparate). The mountainous region also has vegetation and a seasonal snow pack that would cause significant amounts of temporal decorrelation. The maximum mean coherence values $(\gamma_{\text{mean}} \geq 0.7)$ correspond to areas of ground that have large structures on them. These structures produce coherent signals because they do not change over time.

[28] What is most striking about the image shown in Figure 4 is the very regular pattern of the coherent pixels. This regular pattern can be easily seen in Figure 5(a), where we show an enlargement of the area inside the red box in

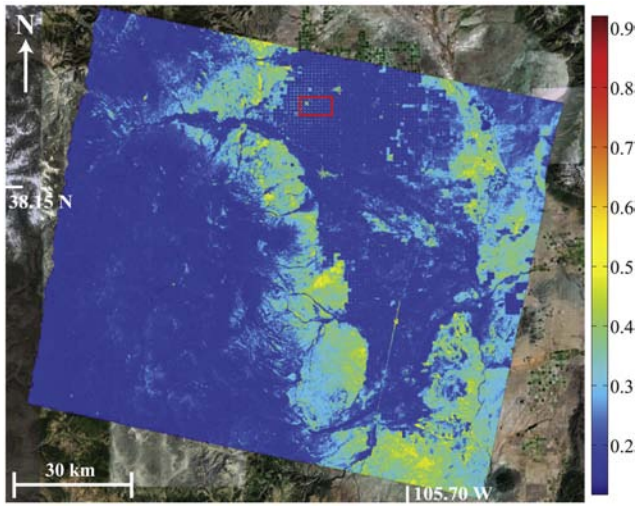

Figure 4. An image of the mean coherence (γ_{mean}), where each pixel corresponds to a 50 m by 50 m area on the ground. The area inside of the red box is enlarged in Figures 5(a) and 5(b) [source of background image: Google Earth map].

Figure 4. The coherent pixels fall on a square grid, with spacing on the order of 800 m. The regions with coherent InSAR data are the interstices between the areas irrigated with the center pivot irrigation systems. Figure 5(b) is a dimmed overlay of the mean coherence image on a map of the area. Figure 5(c) shows the center pivot irrigation system and the circular patterns with interstices. The presence of these areas between the center-pivot fields provides us with the spatial coverage needed to characterize deformation in the SLV. Without these interstices between the center-pivot fields, decorrelation throughout the region would prevent any useful deformation measurements. *Massonnet and Feigl* [1998] saw a similar pattern in a single interferogram. The final step before the inversion, pixel selection, was implemented as described in section 3.2. After pixel selection we computed the SVD LS solution. This provided a time series of the line of sight (LOS) deformation for each selected pixel in the SLV.

4.4. Comparison of LOS Time Series and Hydraulic Head Time Series

[29] The main objective of this study is to determine whether the deformation measurement obtained from the InSAR data in the SLV is of high enough quality to yield useful information about the variation in hydraulic head in the confined aquifer system. Because there were no leveling line surveys performed or extensometers recording deformation in the SLV we are dependent on hydrologic and hydrogeologic data to validate the InSAR measurements in this agricultural area. We will first compare the InSAR deformation measurements to the hydraulic head measurements in monitoring wells; our question being whether we are capturing the expected seasonal variation in head. We will then predict hydraulic head from the InSAR deformation data, using an estimate of S_{ke} from an aquifer test (see equation (1)). We will compare this predicted hydraulic head to the hydraulic head measured in a nearby monitoring well. In order to do this we must find locations where we have high coherence InSAR data, hydraulic head measurements, and estimates of S_{ke} from aquifer tests.

[30] Of the 1500 monitoring wells in the SLV, only 328 sample the confined aquifer system, and only 100 of these have a time series of head measurements over some interval in the time period for which we have InSAR data (1992–2000) [*RGDSS*, 2005]. There have been 151 aquifer tests in the confined aquifer system; however, only 17 of them provide estimates of S [*RGDSS*, 2005]. There are six monitoring well/aquifer test well pairs that were collocated within 2 km of each other. However, upon further inspection it was found that three of the monitoring wells either: (a) did not exhibit seasonal pumping and recharge, or (b) were not sampling the same portion of the aquifer system as the aquifer test wells. We thus had, as our final data set for comparison, hydraulic head measurements from three monitoring wells and three aquifer test wells with estimates of S. We selected the highest coherence pixel within 1 km of the monitoring well to be the location of the line of sight (LOS) deformation measurements. At each of the three monitoring well locations we found that the background phase gradient was low enough to justify a separation of 1 km.

[31] Figures 6(a), 6(c), and 6(e) show the LOS deformation time series for the three high coherence pixels (red markers). The location of each of the deformation time series is labeled as a cyan marker in Figure 7. We have estimated the error in the InSAR measurement to be ~6 mm (shown as error bars in Figure 6). In general little attention is paid to properly quantifying the error in InSAR measurements. We estimated the error in the interferograms by fitting a local plane to the unwrapped phases to account

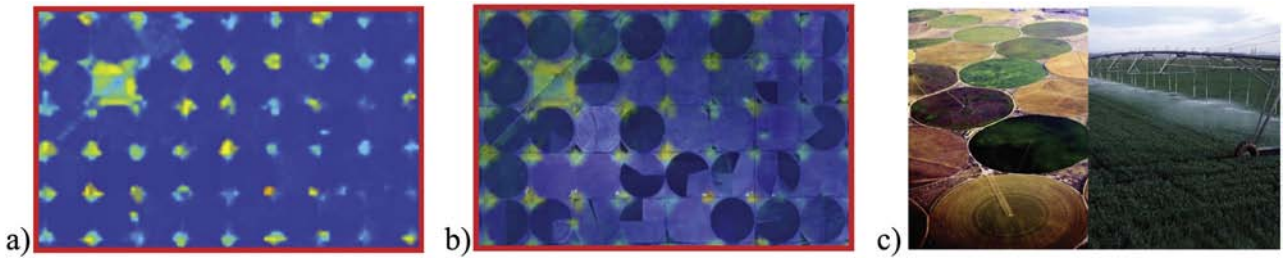

Figure 5. (a) A close-up view of the mean coherence. (b) The mean coherence overlaid on a Google Earth map. The higher coherence areas show up within the interstices between the center-pivot-irrigated areas. (c) Photos of the SLV center-pivot-irrigation fields and watering system (source: thefullwiki.org and agmachine.ning.com).

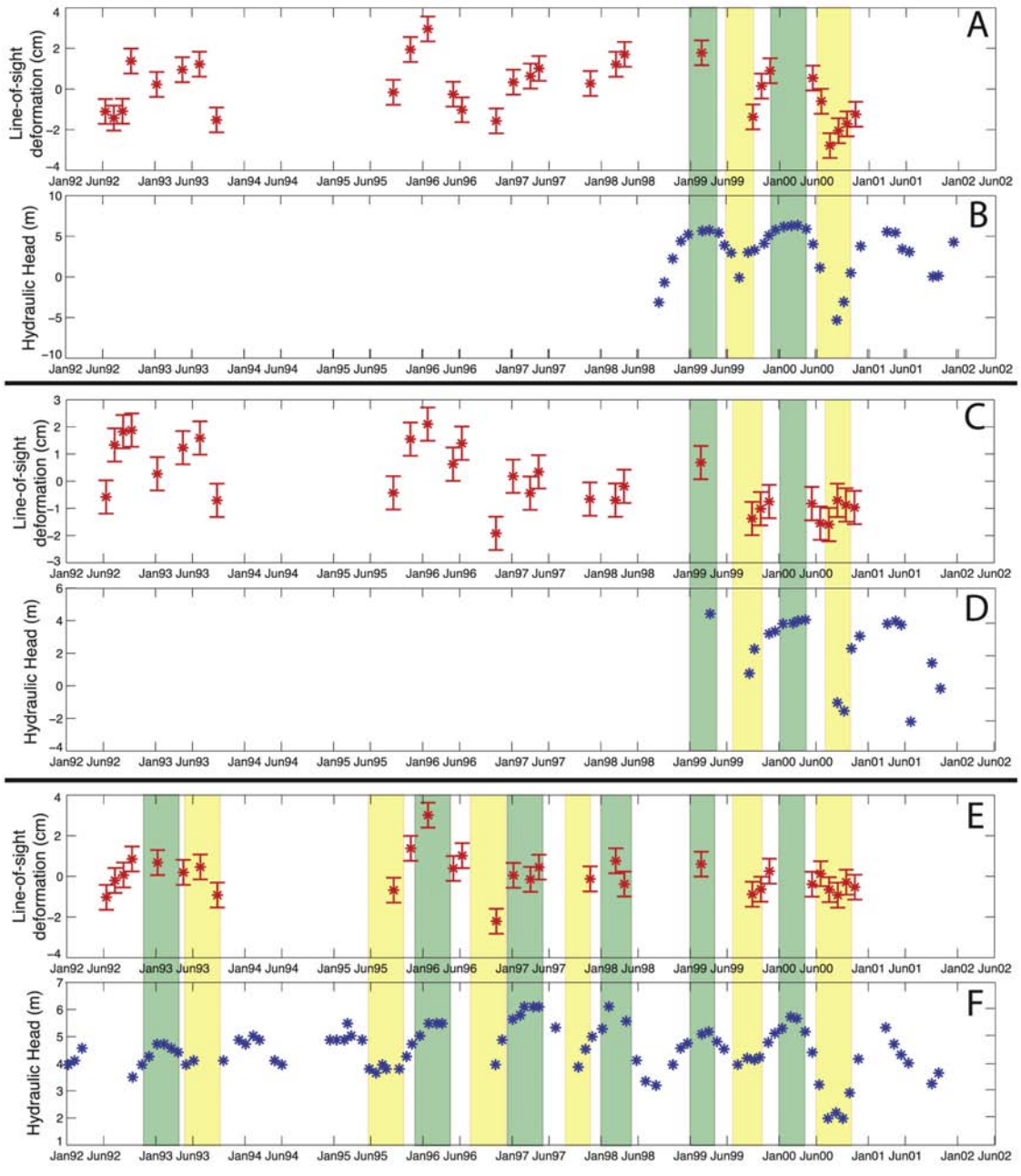

Figure 6. (a), (c), and (e) LOS deformation time series for a high coherence pixel 1 km from ALA6, CON2, and ALA13, respectively. The position of these pixels are shown as cyan markers in Figure 7. (b), (d), and (f) Hydrographs for well ALA6, CON2, and ALA13 respectively. The position of these wells are shown as blue markers in Figure 7. Green highlighted sections show when hydraulic head measurements were high, and yellow show when they were low.

for long-period errors, and then computing the standard deviation of the misfit. This estimate is similar to the error of ~5 mm given by *Hoffman et al.* [2003].

[32] Figures 6(b), 6(d), and 6(f) show the hydraulic head time series for the three monitoring wells: ALA6, CON2, and ALA13, respectively (locations shown as blue markers in Figure 7). In each case the corresponding LOS time series is from the pixel with the highest coherence, within 1 km of the monitoring well. We expect the deformation and hydraulic head to be proportional by the skeletal elastic storage coefficient S_{ke} (equation (1)), and indeed find the two measured time series similarly proportional (Figure 6). We have highlighted in green the times of the year where the hydraulic head in the monitoring well is high, and in yellow the times where the hydraulic head is low. We have done this comparison for times where InSAR and hydraulic head data exist. For all but a few occasions we can see that when the hydraulic head is high, the deformation indicates

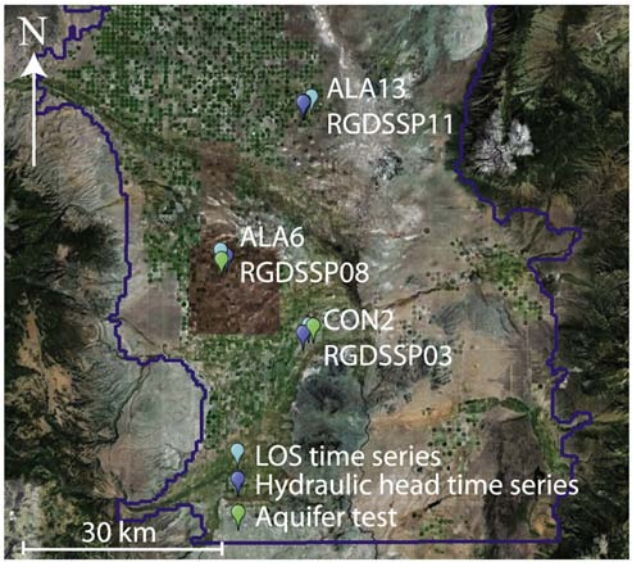

Figure 7. Map of the SLV showing the position of: LOS deformation time series (cyan marker), hydraulic head time series (blue marker), and the aquifer test locations (green marker).

an upward movement of the ground surface, and when the hydraulic head is low, the deformation indicates a downward movement. In general, the agreement of the two time series is better at well ALA6 than at wells CON2 and ALA13. This may be due to the fact that both the hydraulic head change and the deformation are larger at that location. We conclude that the periodicity of the measurements are in good agreement, suggesting that the deformation we are measuring with InSAR in the SLV is recording the seasonal changes in the hydraulic head in the confined aquifer system. This in itself is very useful information that could be used in a qualitative way to indicate when and where significant changes in head occur. In addition, as can be seen in Figure 6, InSAR provides us with data at times before head measurements were being made in many of the wells in the SLV. This longer period of monitoring is valuable for assessing long-term changes in the aquifer. For example, one important observation that can be made is the absence of a significant negative linear trend in the deformation in Figures 6(a), 6(c), and 6(e). This supports the assumption that only elastic deformation is occurring in these regions of the SLV.

4.5. Hydraulic Head Estimate From InSAR and Aquifer Test Data

[33] As a final step, we assessed the accuracy of estimates of hydraulic head that could be derived from InSAR deformation data. We did this by comparing the InSAR-derived Δh to the measured Δh at the three monitoring wells (ALA6, CON2, ALA13). However, in order to make this comparison we needed Δb (InSAR data) and S_{ke} (aquifer test well data) at the monitoring well locations (see equation (1)). We assumed that the deformation measured at the high coherence pixel is approximately the same as the deformation at the monitoring well (~1 km away). The aquifer test wells are: RGDSSP08, RGDSSP03, and RGDSSP11 (locations shown as green markers in Figure 7). The distance between aquifer test wells and monitoring wells is as follows: RGDSSP08 is 300 m from ALA6, RGDSSP03 is 2 km from CON2, and RGDSSP11 is 100 m from ALA13. Although the two wells were collocated within 2 km, if we want to use the estimates of S from the aquifer tests at the monitoring well locations, we need to account for the differences in the thickness of the producing zone for each well, i.e., the thickness of the aquifer from which water is being withdrawn.

[34] During an aquifer test the obtained value of S depends upon the producing zone thicknesses (b^*) at the aquifer test well:

$$S = S_s b^*, \tag{7}$$

where S_s is the specific storage. The monitoring well and aquifer test well pairs were all producing from similar hydrogeologic units, and hence should exhibit similar values of S_s. However, the thickness of the producing zone varied because they were screened over different intervals. In order to use the value of S from the aquifer test well at the monitoring well location we needed to correct for this disparity. The screened interval was used as the producing zone thickness based on the assumption that flow into the well is horizontal: 23.8 m at RGDSSP08, 150.9 m at RGDSSP03, and 75.3 m at RGDSSP11 [*Brendle*, 2002]. We then calculated $S_s = S/b^*$ using the producing zone thicknesses at the aquifer test wells. Using S_s and the producing zone thickness at the monitoring wells: 25.3 m at ALA6, 110.0 m at CON2, and 111.3 m at ALA13, we calculated S at the monitoring wells to be: $S = 1.4 \times 10^{-3}$ for ALA6, $S = 1.7 \times 10^{-3}$ for CON2, and $S = 7.8 \times 10^{-4}$ for ALA13 [*Brendle*, 2002]. As discussed in section 1 of the paper we assumed that the storage from the expansion and contraction of water (S_w) is small and we can use S as a proxy for S_{ke}.

[35] The estimate of S_{ke} at the monitoring well location contains error from two main sources: performing the analytical fit to the recovering hydraulic head measurements and estimating the producing zone thicknesses. While quantification of the error in the analytical fit is not normally performed, the measurements of S_{ke} from the aquifer tests should, in general, be accurate within 10%–20% of the actual value (E. Harmon, personal communication). We have no way of quantifying the error from estimating the producing zone thickness, therefore we neglected to account for it in this study. We used the average of the 10%–20% range, so assumed an error of 0.15 S_{ke}.

[36] Figure 8 shows a comparison of the hydraulic head derived from InSAR measurements and the hydraulic head measurements. In general, the hydraulic head is overestimated when compared to the measured hydraulic head. This suggests that the values for S_{ke} derived from the aquifer test may be underestimated. This may be due to the uncertainty involved in identifying the producing zone thickness. The error bars on the InSAR-derived head estimates contain both the 15% relative error in S_{ke} and the 0.6 cm error in the deformation measurement and were calculated as follows:

$$\delta h = \Delta h \sqrt{\left(\frac{\delta b^2}{\Delta b}\right) + \left(\frac{\delta S_{ke}^2}{S_{ke}}\right)}, \tag{8}$$

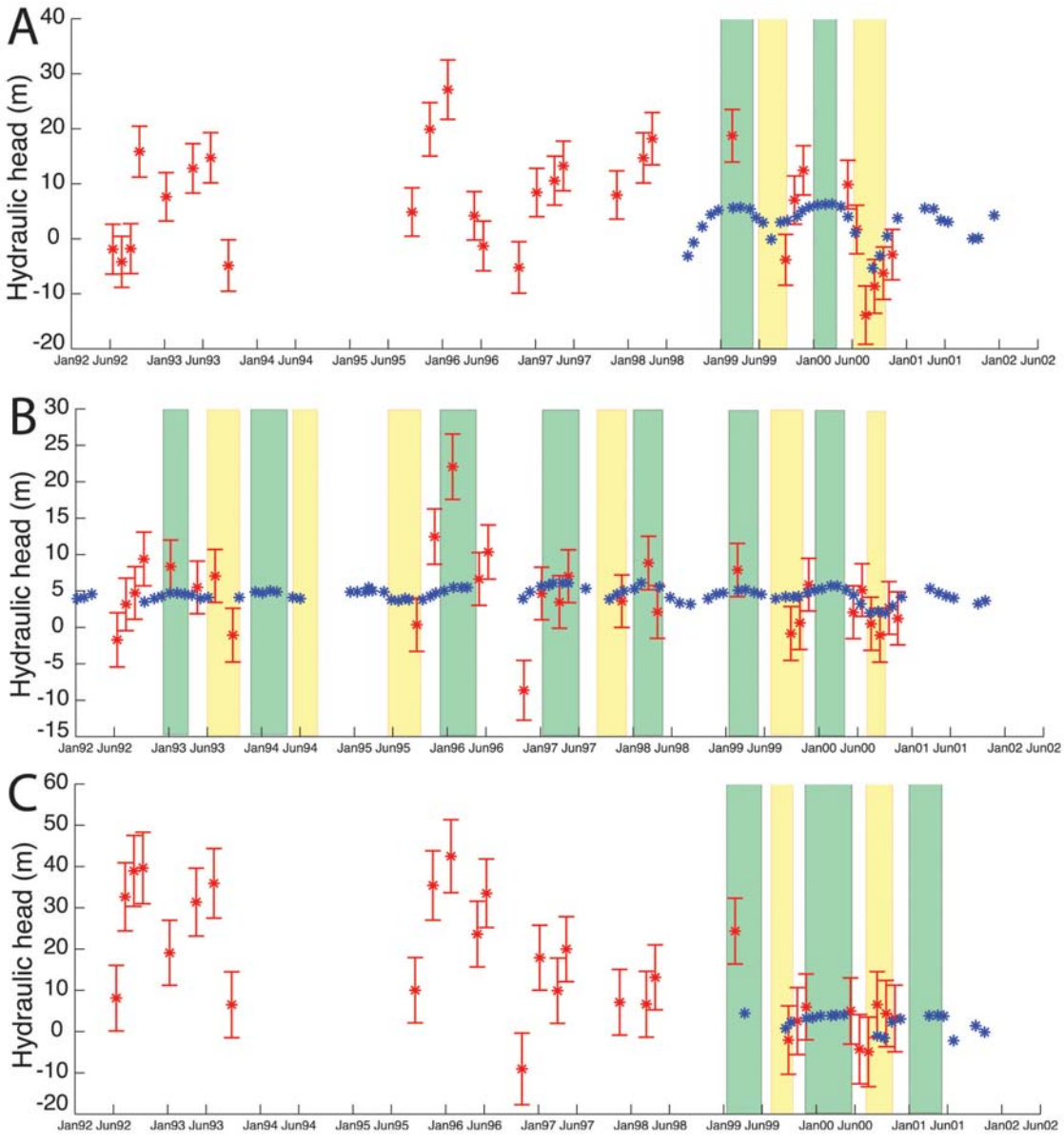

Figure 8. Estimated (red markers) and measured hydraulic head (blue markers). (a) ALA6, (b) CON2, and (c) ALA13. Green highlighted sections show when hydraulic head measurements were high, and yellow show when they were low.

where δb is the error in Δb, δS_{ke} is the error in S_{ke}, and δh is the error in Δh. We found that the error bars were large: approximately ± 4.5, $\pm$ 3.5, and ± 8 m at ALA6, CON2, and ALA13, respectively.

[37] In all three of the plots in Figure 8 we see that in many instances the measured hydraulic head falls within the error bars of the estimated hydraulic head values. At well ALA6, 5 of the 10 InSAR-derived head estimates fall within the error bars of the measured values; at well CON 2, 20 of 31 agree; and at ALA13, 9 of 10 agree. However, as discussed earlier, the error bars we calculated were very large compared to the hydraulic head changes measured in the monitoring wells. In order to make this method of estimating hydraulic head more viable in the future we will need to develop a better way to quantitatively link the InSAR deformation measurement to a head measurement. This will include improving our ability to accurately determine the uncertainty in both S from aquifer tests as well as δb from the InSAR measurements.

[38] A number of spurious points occur in the InSAR-derived head estimates: in February we see a large amount of upward deformation and in November 1996 we see a large amount of downward deformation. Because we did not filter the LOS deformation time series temporally there is still a chance that atmospheric noise could be the cause of these outliers.

5. Conclusions

[39] Our first finding of significance in this study was the discovery that many of the small areas, left unwatered by the center-pivot irrigation systems, yield high quality

InSAR data when processed using SBAS methods. We then found that the InSAR deformation measurements showed the same seasonal periodicity seen in hydraulic head data from monitoring wells. When we attempted to estimate head from the InSAR data, we found good agreement within the error bars with the measured head values. However, we acknowledge that the errors are so large that these head measurements derived from InSAR alone would not provide the level of accuracy required for modeling the confined aquifer system in the SLV. It is clear that more research is required to understand how best to predict head from InSAR data. Can this be done using the field measurements of S_{ke} if we can improve the accuracy of the measurement? Or should we assume that the use of InSAR data to obtain head estimates will always require calibration, with wells in selected regions instrumented specifically for this purpose?

[40] Despite the fact that we cannot yet accurately obtain hydraulic head estimates from the InSAR data, we conclude that we can obtain high quality InSAR data from the SLV, and that these data capture useful information about the seasonal variability in head. These encouraging results lead us to suggest that InSAR data be processed using SBAS for all locations in the SLV where the mean coherence is high. Once we do determine how to accurately obtain head from InSAR data, it is easy to see from Figure 8 that a host of new data will become available to water managers. For example, at ALA6 and ALA13, where hydraulic head data have only been collected since 1999, we will be able to provide estimates of hydraulic head back to 1992. Our hope is that InSAR data from this region can also be used going forward as an integral part of hydrogeologic modeling and monitoring in the valley. In anticipation of this we submitted a proposal to the WInSAR consortium, requesting InSAR coverage of the SLV. Our proposal was approved, the result being that the ERS-2 satellite regularly collected data over the SLV from September 2008–July 2011 when the ERS-2 satellite was decommissioned. By combining the ERS-1/2 measurements with those from the Envisat satellite, acquired from 2002 to 2010, there is the potential for the past records to fill in temporal and spatial data gaps in poorly sampled areas of the SLV.

[41] We see InSAR as providing a new way to complement expensive and spatially sparse aquifer tests and monitoring with a more economical method of collecting field data. The incorporation of InSAR data could be an affordable way to centralize systems for monitoring and modeling of groundwater aquifers. As recently done in California with the passage of Senate Bill 6, it is likely that legislation will be put in place in many western states with requirements to monitor and report hydraulic head. With further development, we are optimistic that InSAR could provide the measurements to cost effectively meet the needs of such legislation, thus facilitating the implementation and adoption of the legislation. If we are to use monitoring of groundwater aquifers to effectively meet the global challenge of managing our groundwater resources, we need robust, reliable, cost-effective forms of monitoring. InSAR and other satellite-based methods of data acquisition, have great potential to address this need, thus leading to improved methods of groundwater management.

[42] **Acknowledgments.** We are grateful to Eric Harmon of HRS Water Consultants Inc. for his assistance with this work. We would like to thank UNAVCO for access for to their WInSAR and Geoearthscope SAR archives. This research was supported primarily by a Nelson award to Jessica Reeves from the Department of Geophysics at Stanford University, with additional support through funding to R. Knight from Schlumberger Water Services.

References

Amelung, F., D. L. Galloway, J. W. Bell, H. A. Zebker, and R. J. Laczniak (1999), Sensing the ups and downs of Las Vegas: InSAR reveals structural control of land subsidence and aquifer-system deformation, *Geo*, *27*(6), 483–486.

Berardino, P., G. Fornaro, R. Lanari, and E. Sansosti (2002), A new algorithm for surface deformation monitoring based on small baseline differential SAR interferograms, *IEEE Trans. Geosci. Remote Sens.*, *40*(11), 2375–2383.

Brendle, D. (2002), *Geophysical logging to determine construction, contributing zones, and appropriate use of water levels measured in confined-aquifer network wells, San Luis Valley, Colorado*, 1998–2000, edited by U. S. G. Survey, Denver, Colorado.

Canuti, P., N. Casagli, P. Farina, A. Ferretti, F. Marks, and G. Menduni (2006), Analysis of subsidence phenomena in the Arno river basin using radar interferometry, *Giornale Geolog. Appl.*, *4*, 131–136.

Chen, C. W., and H. Zebker (2002), Phase unwrapping for large SAR interferograms: statistical segmentation and generalized network models, *ITGRS*, *40*(8), 1709–1719.

Ferretti, A., C. Prati, and F. Rocca (2000), Nonlinear subsidence rate estimation using permanent scatterers in differential SAR interferometry, *ITGRS*, *38*(5), 2202–2212.

Ferretti, A., C. Prati, and F. Rocca (2001), Permanent scatterers in SAR interferometry, *ITGRS*, *39*(1), 8–20.

Ferretti, A., A. Monti-Guarnieri, C. Prati, F. Rocca, and D. Massonnet (2007), *InSAR Principles: Guidelines for SAR Interferometry Processing and Interpretation*, edited by E. S. Agency, ESA, Frascati, Italy.

Galloway, D. L., and J. Hoffmann (2007), The application of satellite differential SAR interferometry-derived ground displacements in hydrogeology, *Hyd. J.*, *15*, 133–154, doi:10.1007/s10040-006-0121-5.

Galloway, D. L., K. W. Hudnut, S. E. Ingebritsen, S. P. Phillips, and G. Peltzer (1998), Detection of aquifer system compaction and land subsidence using interferometric synthetic aperture radar, Antelope Valley, Mojave Desert, California, *Water Resour. Res.*, *34*(10), 2573–2585.

Hanssen, R. F. (2001), *Radar Interferometry – Data Interpretation and Error Analysis*, Kluwer, Dordrecht, Netherlands.

Hoffmann, J., H. Zebker, D. Galloway, and F. Amelung (2001), Seasonal subsidence and rebound in Las Vegas Valley, Nevada, observed by synthetic aperture radar interferometry, *Water Resour. Res.*, *37*(6), 1551–1566.

Hoffmann, J., D. L. Galloway, and H. A. Zebker (2003), Inverse modeling of interbed storage parameters using land subsidence observations, Antelope Valley, California, *Water Resour. Res.*, *39*(2), 1031, doi:10.1029/2001WR001252.

Larsen, Y., G. Engen, T. R. Lauknes, E. Malnes, and K. A. Hogda (2005), A generic differential InSAR processing system, with applications to land subsidence and SWE retrieval, paper presented at Advances in SAR Interferometry from ENVISAT and ERS missions (Fringe 2005), ESA ESRIN, Frascati, Italy, 28 November–2 December.

Lauknes, T. R. (2004), Long-term surface deformation mapping using small-baseline differential SAR interferograms, C.Sc. thesis, Fac. of Sci., Dep. of Phys., Univ. of Tromso, Tromso, Norway.

Massonnet, D., and K. L. Feigl (1998), Radar interferometry and its application to changes in the Earth's surface, *Rev. Geophys.*, *36*(4), 441–500.

Meyer, B., R. Armijo, D. Massonnet, J. B. d. Chabalier, C. Delacourt, J. C. Ruegg, J. Achache, P. Briole, and D. Papanastassiou (1996), The 1995 Grevena (Northern Greece) Earthquake: Fault model constrained with tectonic observations and SAR interferometry, *Geo. RL*, *23*(19), 2677–2680.

RGDSS (2005), Rio Grande Decision Support System Groundwater Model as of 29 July 2005, Principia Mathematica, Lakewood, Colorado.

Riley, F. S. (1969), Analysis of borehole extensometer data from central California, *Int. Assoc. Sci. Hydrol. Publ.*, *89*, 423–431.

Schmidt, D. A., and R. Burgmann (2003), Time-dependent land uplift and subsidence in the Santa Clara valley, California, from a large interferometric synthetic aperture radar data set, *J. Geophys. Res.*, *108*(B9), 2416, doi:10.1029/2002JB002267.

Todd, D. K. (1980), *Groundwater Hydrology*, 2nd ed., John Wiley, New York.

Watson, K. M., Y. Bock, and D. T. Sandwell (2002), Satellite interferometric observations of displacements associated with seasonal groundwater in the Los Angeles basin, *J. Geophys. Res.*, *107*(B4), 2074, doi:10.1029/2001JB000470.

Wisely, B. A., and D. A. Schmidt (2010), Deciphering vertical deformation and poroelastic parameters in a tectonically active fault-bound aquifer using InSAR and well level data, San Bernardino basin, California, *Geophys. J. Int.*, *181*, 1185–1200, doi:10.1111/j.1365-246X.2010.04568.x

Zebker, H., and J. Villasenor (1992), Decorrelation in interferometric radar echoes, *ITGRS*, *30*(5), 950–959.

Zebker, H., C. L. Werner, P. A. Rosen, and P. Hensley (1994), Accuracy of topographic maps derived from ERS-l interferometric radar, *ITGRS*, *32*(4), 823–836.

Zebker, H., P. A. Rosen, and P. Hensley (1997), Atmospheric effects in interferometric synthetic aperture radar surface deformation and topographic maps, *JGR*, *102*(B4), 7547–7563.

R. Knight, J. A. Reeves, and H. A. Zebker, Department of Geophysics, Stanford University, 397 Panama Mall, Stanford, CA 94305, USA. (rknight@stanford.edu; jesser@stanford.edu; zebker@stanford.edu)

T. R. Lauknes, Northern Research Institute (Norut), P. O. Box 6434, Tromsø Science Park, NO-9294 Tromsø, Norway. (tom.rune.lauknes@norut.no)

W. A. Schreüder, Principia Mathematica, 445 Union Blvd #230, Lakewood, CO 80228, USA. (Willem.Schreuder@prinmath.com)

P. Shanker Agram, Division of Geological & Planetary Sciences, California Institute of Technology, 1200 E. California Blvd., Pasadena, CA 91125, USA. (shanker@caltech.edu)